



The two types of El-Niño and their impacts on the length of day

O De Viron, Jean O. Dickey

► **To cite this version:**

O De Viron, Jean O. Dickey. The two types of El-Niño and their impacts on the length of day. *Geophysical Research Letters*, American Geophysical Union, 2014, 41, pp.3407 - 3412. <10.1002/2014GL059948>. <hal-01087222>

HAL Id: hal-01087222

<https://hal.archives-ouvertes.fr/hal-01087222>

Submitted on 26 Nov 2014

HAL is a multi-disciplinary open access archive for the deposit and dissemination of scientific research documents, whether they are published or not. The documents may come from teaching and research institutions in France or abroad, or from public or private research centers.

L'archive ouverte pluridisciplinaire **HAL**, est destinée au dépôt et à la diffusion de documents scientifiques de niveau recherche, publiés ou non, émanant des établissements d'enseignement et de recherche français ou étrangers, des laboratoires publics ou privés.

1 The two types of El-Niño and their impacts on the Length-of-day

O. de Viron and J. O. Dickey

2 At the interannual to decadal timescale, the changes in
3 the Earth rotation rate are linked with the El-Niño South
4 ern Oscillation phenomena through changes in the Atmo-
5 spheric Angular Momentum. As climatic studies demon-
6 strate that there were two types of El-Niño events, namely
7 Eastern Pacific (EP) and Central Pacific (CP) events, we in-
8 vestigate how each of them affect the Atmospheric Angular
9 Momentum. We show in particular that EP events are asso-
10 ciated with stronger variations of the Atmospheric Angular
11 Momentum and length-of-day. We explain this difference
12 by the stronger pressure gradient over the major mountain
13 ranges, due to a stronger and more efficiently localized pres-
14 sure dipole over the Pacific Ocean in the case of EP events.

1. Introduction

15 The Earth rotation is not constant in time; in particular
16 the Earth rotation rate, and the associated length-of-day
17 (LOD) show fluctuations in a broad band of periods. A
18 global description of the causes at the different time scales
19 can be found in *Hide and Dickey* [1991]. The main cause of
20 LOD change for periods ranging from a few days to a few
21 years is the Earth atmosphere interaction. As soon as in-
22 terannual fluctuations were observed in the Earth rotation
23 data, the El-Niño Southern Oscillation (ENSO) was shown
24 to play a major role [*Chao*, 1984, 1988], as a warm – El-Niño
25 – event has been shown associated with a longer day and a
26 cold – La Niña – event associated with a shorter day.

27 Classical El-Niño events are characterized by maximum
28 warm water anomaly in the Eastern Pacific Ocean, and re-
29 ferred as the Eastern Pacific (EP) El-Niño events, with Sea
30 Surface Temperature (SST) anomalies in the Niño-3 region
31 (5° S - 5° N, 150° W to 90° W). Frequent occurrences of a
32 new type of El Niño have been observed since the 1990s, with
33 the maximum warm SST anomaly in the Central Equatorial
34 Pacific [e.g. *Latif et al.*, 1997], the Niño-4 region (5° S - 5°
35 N, 160° E to 150° W). These are known with a variety of
36 names, Central Pacific (CP) El Niño [*Kao and Yu*, 2009; *Yü*
37 *and Kim*, 2010], warm pool El Niño [*Kug et al.*, 2009], date
38 line El Niño [*Larkin and Harrison*, 2005] or El Niño Modoki
39 [*Ashok et al.*, 2007]. These two ENSO types have differ-
40 ent teleconnection patterns and climatic consequences [e.g.
41 *Weng et al.*, 2009; *Kim et al.*, 2009; *Ashok and Yamagata*,
42 2009; *Kim et al.*, 2009]. In this study, we investigate how
43 the EP and CP event mechanisms affect the Earth rotation
44 differently.

Classically, the atmospheric impact on the Earth rota-
tion is estimated using the angular momentum (AM) ap-
proach: the solid Earth+atmosphere system is considered
as isolated, the atmospheric angular momentum (AAM) is
computed, considering that any variation of this quantity
is compensated by an opposite variation of the Earth AM.
The AAM is composed of two parts, a mass term corre-
sponding to the AM associated with the rigid rotation of
the atmosphere with the solid Earth, and a motion term
corresponding to the relative AM of the atmosphere with
respect to the solid Earth.

Alternatively, as first proposed by *Widger* [1949], one can
also consider the atmosphere as an external forcing to the
solid Earth. The total atmospheric torque acting on the
solid Earth is the sum of four effects: a pressure effect on the
topography, the gravitational interaction between the atmo-
spheric and the Earth masses, the wind friction drag over the
Earth surface, and the interaction between the gravity wave
and the topography [*Barnes et al.*, 1983; *Huang et al.*, 1999].
The last term is generally negligible [*de Viron and Dehant*,
2003]. The topography from the atmospheric Global Circu-
lation Models (GCMs) is classically defined with respect to
the geoid; consequently, the topographic torque computed
using such a topography is actually the sum of topogra-
phy and gravitational torque, and is known as the mountain
torque. The total torque is thus computed as the sum of the
mountain and the friction torque.

Generally, the mountain torque generates the axial AAM
variations, which are eventually damped away by the friction
torque [*de Viron et al.*, 2001; *Lott et al.*, 2008; *Marcus et al.*,
2011]. A noticeable exception is the seasonal AAM anomaly,
which is generated by an anomalous friction torque over the
Indian Ocean [*de Viron et al.*, 2002]. Both the atmospheric
AM (AAM) and torques can be estimated from the output,
whereas the inherent accuracy limits this method at the un-
derstanding of the physical processes but does not allow to
estimate Earth rotation variation with a precision allowing
to use it in the frame of geodetic studies [*de Viron and De-*
hant, 2003].

The torque approach was used for understanding the
atmospheric angular momentum anomaly associated with
the ENSO phenomenon [*Wolf and Smith*, 1987; *Ponte and*
Rosen, 1999; *de Viron et al.*, 2001; *Marcus et al.*, 2010]. Dur-
ing the ENSO event, a low pressure appears in the Eastern
part of the Pacific Ocean, which creates a positive torque
over the atmosphere and consequently increases the AAM
and the LOD. The increased surface wind over the North-
ern Pacific increases the friction torque, which eventually
cancels the AAM anomaly.

2. Data Preparation

49 In this study, we used outputs of the National Centers
50 for Environmental Prediction – National Center for Atmo-
51 spheric Research (NCEP-NCAR) reanalysis [*Kalnay et al.*,
52 1996], from 1948 to 2013. Data includes the zonal wind
53 field (as a function of time, pressure level, latitude, and lon-
54 gitude), the surface pressure and East-West wind stress (as
55 a function of time, latitude, and longitude), and the model
56 orography.

¹Université Paris Diderot, Sorbonne Paris Cité, and
Institut de Physique du Globe de Paris (UMR7159), now at
Univ La Rochelle, CNRS, UMR 7266, Littoral
Environnement & Société LIENSs, F-17000 La Rochelle,
France

²Jet Propulsion Laboratory, California Institute of
Technology, Pasadena, CA

102 The Z component of the AAM is estimated from

$$H_Z^{\text{motion}} = \frac{a^3}{g} \int_0^{2\pi} \int_0^\pi \int_0^{P_{\text{surface}}} u(p, \theta, \lambda) \sin^2 \theta dp d\theta d\lambda \quad (1)$$

$$H_Z^{\text{mass}} = \frac{a^4 \Omega}{g} \int_0^{2\pi} \int_0^\pi P_{\text{surface}}(\theta, \lambda) \sin^3 \theta d\theta d\lambda, \quad (2)$$

103 where a is the mean Earth radius, g is the mean gravity
104 acceleration, u is the zonal wind, P_{surface} is the surface pres-
105 sure, θ and λ are the colatitude and longitude, and Ω is the
106 Earth mean angular velocity. In order to be able to investi-
107 gate the space pattern of the anomaly, we also used the
108 expression of equation (1) only integrated along the longi-
109 tude, corresponding to the contribution to the motion term
110 at a given latitude, pressure level, and time.

111 The axial torque are estimated from the surface pressure
112 longitude derivative and orography using

$$\Gamma_Z^{\text{Mountain}} = a^3 \int_0^{2\pi} \int_0^\pi \frac{\partial P_{\text{surface}}(\theta, \lambda)}{\partial \lambda} h(\theta, \lambda) \sin \theta d\theta d\lambda \quad (3)$$

$$\Gamma_Z^{\text{Friction}} = -a^3 \int_0^{2\pi} \int_0^\pi \tau_\lambda \sin^2 \theta d\theta d\lambda, \quad (4)$$

where h is the orography and τ_λ is the zonal friction drag.
The longitude derivative of the surface pressure is estimated
using a using a five-point stencil [e.g. *Burden and Faires*,
2010]:

$$\left. \frac{df(x)}{dx} \right|_i \simeq \frac{8f_{i-2} - f_{i-1} + f_{i+1} - 8f_{i+2}}{12 \Delta x} \quad (5)$$

The EP and CP Niño index are estimated, following *Rebo*
and Jin [2011], from the Niño 3 and Niño 4 index from the
NOAA Climate Prediction Center, made available at the
Earth System Research Laboratory website. Defining

$$\alpha = \begin{cases} \frac{2}{5} \\ 0 \end{cases} \text{ where } \text{Nino}_3 \cdot \text{Nino}_4 < 0$$

$$N_{EP} = \text{Nino}_3 - \alpha \cdot \text{Nino}_4 \quad (6)$$

$$N_{CP} = \text{Nino}_4 - \alpha \cdot \text{Nino}_3 \quad (7)$$

113 To minimize the impact of the high-frequency noise in the
114 computation, the indices are smoothed by a 1-year running
115 mean. We isolate the impact of each type of events by first
116 separating the data epochs into three categories, for each
117 index, the epochs with index values above 1σ being the pos-
118 itive state, with index values below -1σ being the negative
119 state, and the value in the interval $[-\sigma, \sigma]$ being the neutral
120 state.

$$t_X^+ = \{t : N_X(t) > \sigma_{N_X}\} \quad (8)$$

$$t_X^0 = \{t : -\sigma_{N_X} \leq N_X(t) \leq \sigma_{N_X}\} \quad (9)$$

$$t_X^- = \{t : N_X(t) < -\sigma_{N_X}\} \quad (10)$$

We then compute a composite anomaly by making the dif-
ference between the average positive state and the average
negative state.

$$C_X(x, y) = \overline{C(t_X^+, x, y)} - \overline{C(t_X^-, x, y)} \quad (11)$$

121 where X can be either EP or CP , and $C(t, x, y)$ is the
122 dataset at time t and coordinates (x, y) .

3. ENSO induced AAM anomaly

We estimated the composite impact of the ENSO by com-
puting the mean AAM for $t_{EP}^{+,0,-}$ and $t_{CP}^{+,0,-}$. Whisker dia-
grams for each of them are plotted on Figure 1, the as-
sociated AAM anomaly can be observed on the left axis,
whereas the corresponding LOD anomaly can be read on
the right axis. The above average values of both EP and
CP indices are seen to be associated with anomalously high
value of AAM, whereas below average index values are asso-
ciated with anomalously low value of AAM. The difference
is found significant at more than 99% with an ANOVA test
(see *Davis* [1986], for example). The t_X^0 are the largest set,
with about 500 epochs, whereas the + and - have about 100.
Due to the one-year smoothing, the epochs from the same
winter are not independents; consequently, for the statis-
tics, only the mean value over a given winter was kept. The
ANOVA group size was subsequently of the order of 15 to
20 winters for the + and - epochs, and about 100 for the 0
epochs.

The EP anomaly is stronger: in particular, the difference
of mean between above average and below average is nearly
2.5 time larger for EP than for CP.

4. AAM and torque for the two types of ENSO events

Such a difference in AAM signature finds its explana-
tion in the torque acting on the atmosphere from the solid
Earth. As explained in *Ponte and Rosen* [1999], the torque
causing the AAM anomaly in the case of an ENSO event is
the mountain torque associated with the pressure anomaly.
The Southern Oscillation is known (see for instance *Clarke*
[2008]) to be associated with a pressure East-West dipole
over the Pacific. However, depending on the type of events,
the location of this dipole is directly linked to that of the SST
anomaly, as shown on Figure 2. In particular, the EP neg-
ative pole is centred on the east coast of the Pacific Ocean,
whereas the WP negative pole is centred on the middle of
the Pacific Ocean.

The mountain torque is generated by a longitude differ-
ence of pressure acting over a mountain range: if the pres-
sure over the West slope of the mountain is stronger than
that over the East side, it acts to push the Earth to ro-
tate faster and slows the atmosphere rotation down. Con-
sequently, to understand the impact of the ENSO events
on the AAM, mostly the pressure over the main mountain
ranges, Himalayas, Andes, and Rocky Mountains are rele-
vant.

The Figure 3 focus over those three mountain ranges,
showing the topography in a gray scale, and the pressure
anomaly with color contours. The most obvious difference
occurs over Himalayas: in case of the EP ENSO, there is a
strong pressure gradient with the pressure on the West slope
being smaller, whereas there is no such gradient in case of
CP ENSO. Over the Andes, a pressure gradient exists in
both cases, but it is shifted East in the case of CP ENSO,
and is consequently not acting over topography, while the
gradient in case of EP ENSO closely follows the coast, and
the mountain range, and is consequently very efficient. Over
the Rocky Mountains, a pressure gradient on the West slope
can be noted in both cases, but the more westward location
of the pressure dipole for the CP events makes it weaker.
Consequently, the mountain torque associated with the EP
ENSO is stronger in all the three cases. The values of the

mountain torque, total and integrated over each continent
are given on Table 1. The table shows that there is also
some effect over the topography of Africa.

The friction torque shows similar features in case of CP
and EP ENSO, but they are stronger in the case of the EP
ENSO. The anomaly maps are shown on Figure 4. The total
friction torque is at the level of 10 Hadleys for EP ENSO
and about a third for CP ENSO, with maximum effect over
the Pacific and over the part of the Antarctic Ocean, North
of the Indian Ocean, as seen on Table 2. The stronger fric-
tion in the case of EP ENSO is logical, considering that the
wind anomaly is stronger in the CP ENSO case. A stronger
friction torque is also necessary to break down the larger
AAM anomaly resulting from the larger mountain torque in
the EP ENSO case.

5. Conclusions

In this paper, we investigate the impact of the ENSO on
the Earth rotation, and show that the AAM signature of the
Eastern Pacific type of ENSO is more than twice as large
than that of the Central Pacific ENSO. We then explain this
difference using the torque approach, as it allows us to de-
termine where and how the AM is exchanged between the
solid Earth and the atmosphere. As expected, we also find
stronger torques for the EP ENSO, for both the mountain
and the friction torque. The ratio of the dominant mountain
torque created by the Eastern Pacific events to that created
by the Central Pacific events varies between 1.5 and 3.0,
with the ratio on the total mountain torque being 2.6. The
strongest contributing continents are Asia, North and South
America and Africa. For the frictional torque, this ratio is
3.0. Looking at the associated surface pressure anomaly, we
show that the pressure dipole for EP ENSO is positioned
so that there is a strong East-West pressure gradient
over the major mountain ranges: Himalayas, Andes, Rocky
Mountains, whereas the pressure dipole for CP ENSO is
not as efficiently positioned. The stronger mountain torque
explains the stronger AAM anomaly. The stronger wind as-
sociated with the anomaly generate a stronger negative fric-
tion torque at the Earth surface, which cancels the AAM
anomaly.

This case study demonstrates how the torque approach
provides additional insights, explaining the AAM changes.
In this case, it allows to provide an explanation as why the
two types of ENSO events do not have the same impact on
the Earth rotation.

Acknowledgments. We gratefully acknowledge discussions
with Tong Lee regarding the two ENSO type literatures. This
study was supported by the CNES through the TOSCA program
and by the Institut Universitaire de France (OdV). The work
JOD is a phase of research carried out at the Jet Propulsion
Laboratory, California Institute of Technology, sponsored by the
National Aeronautics and Space Administration (NASA). It is
pleasure to thank the editor (Eric Calais) and two anonymous
reviewers for their help in improving the paper.

References

Ashok, K., and T. Yamagata (2009), Climate Change The
Nino with a difference, *Nature*, 461(7263), 481–484, doi:
10.1038/461481a.
Ashok, K., S. K. Behera, S. A. Rao, H. Weng, and T. Yamagata
(2007), El Nino Modoki and its possible teleconnection, *J.
Geophys. Res.-Ocean*, 112(C11), doi:10.1029/2006JC003798.
Barnes, R., R. Hide, A. White, and C. Wilson (1983), Atmo-
spheric angular momentum fluctuations, length-of-day changes
and polar motion, *Proceedings of the Royal Society of London
A. Mathematical and Physical Sciences*, 387(1792), 31–73.

Burden, R., and J. Faires (2010), *Numerical Analysis*, Cengage
Learning.
Chao, B. (1984), Interannual length-of-day variation with rela-
tion to the Southern Oscillation/El-Nino, *Geophys. Res. Lett.*,
11(5), 541–544, doi:10.1029/GL011i005p00541.
Chao, B. F. (1988), Correlation of Interannual Length-of-Day
Variation With El-Niño/Southern Oscillation, 1972-1986, *Jo.
of Geophys. Res.*, 93(B7), 7709–7715.
Clarke, A. (2008), *An Introduction to the Dynamics of El Nino
& the Southern Oscillation*, Elsevier Science.
Davis, J. (1986), *Statistics and Data Analysis in Geology*, John
Wiley & Sons.
de Viron, O., and V. Dehant (2003), Tests on the validity of at-
mospheric torques on earth computed from atmospheric model
outputs, *J. of Geophys. Res.*, 108(B2), 2068.
de Viron, O., S. Marcus, and J. Dickey (2001), Atmospheric
torques during the winter of 1989: Impact of ENSO and NAO
positive phases, *Geophys. Res. Lett.*, 28(10), 1985–1988.
de Viron, O., J. O. Dickey, and S. L. Marcus (2002), Annual at-
mospheric torques: Processes and regional contributions, *Geo-
phys. Res. Lett.*, 29(7), 44–1–44–3, doi:10.1029/2001GL013859.
de Viron, O., S. Marcus, and J. Dickey (2001), Atmospheric
torques during the winter of 1989: Impact of ENSO and NAO
positive phases, *Geophys. Res. Lett.*, 28(10), 1985–1988.
Hide, R., and J. O. Dickey (1991), Earth’s variable rotation, *Sci-
ence*, 253, 629–637.
Huang, H., P. Sardeshmukh, and K. Weickmann (1999), The
balance of global angular momentum in a long-term atmo-
spheric data set, *Journal of Geophysical Research: Atmo-
spheres*, 104(D2), 2031–2040, doi:10.1029/1998JD200068.
Kalnay, E., M. Kanamitsu, R. Kistler, W. Collins, D. Deaven,
L. Gandin, M. Iredell, S. Saha, G. White, J. Woollen,
Y. Zhu, M. Chelliah, W. Ebisuzaki, W. Higgins, J. Janowiak,
K. Mo, C. Ropelewski, J. Wang, A. Leetmaa, R. Reynolds,
R. Jenne, and D. Joseph (1996), The NCEP/NCAR 40-year
reanalysis project, *Bull. Am. Met. Soc.*, 77(3), 437–471, doi:
10.1175/1520-0477(1996)077.
Kao, H.-Y., and J.-Y. Yu (2009), Contrasting Eastern-Pacific and
Central-Pacific Types of ENSO, *J. of Clim.*, 22(3), 615–632,
doi:10.1175/2008JCLI2309.1.
Kim, H.-M., P. J. Webster, and J. A. Curry (2009), Impact
of Shifting Patterns of Pacific Ocean Warming on North
Atlantic Tropical Cyclones, *Science*, 325(5936), 77–80, doi:
10.1126/science.1174062.
Kug, J.-S., F.-F. Jin, and S.-I. An (2009), Two Types of El Nino
Events: Cold Tongue El Nino and Warm Pool El Nino, *J.
Clim.*, 22(6), 1499–1515, doi:10.1175/2008JCLI2624.1.
Larkin, N., and D. Harrison (2005), Global seasonal temperature
and precipitation anomalies during El Nino autumn and winter,
Geophys. Res. Lett., 32(16), doi:10.1029/2005GL022860.
Latif, M., R. Kleeman, and C. Eckert (1997), Greenhouse warm-
ing, decadal variability, or El Nino? An attempt to under-
stand the anomalous 1990s, *J. of Clim.*, 10(9), 2221–2239,
doi:10.1175/1520-0442(1997)010<2221:GWDVOE>2.0.CO;2.
Lott, F., O. De Viron, P. Viterbo, and F. Vial (2008), Axial atmo-
spheric angular momentum budget at diurnal and subdiurnal
periodicities, *J. Atm. Sc.*, 65(1), 156–171.
Marcus, S. L., O. de Viron, and J. O. Dickey (2010), Interannual
atmospheric torque and El Niño–Southern Oscillation: Where
is the polar motion signal?, *J. of Geophys. Res.*, 115(B12),
B12,409.
Marcus, S. L., O. de Viron, and J. O. Dickey (2011), Abrupt
atmospheric torque changes and their role in the 1976-1977
climate regime shift, *J. of Geophys. Res.-Atmosphere*, 116,
doi:10.1029/2010JD015032.
Ponte, R. M., and R. D. Rosen (1999), Torques responsible for
evolution of atmospheric angular momentum during the 1982-
83 El Niño, *J. of the Atm. Sci.*, 56(19), 3457–3462.
Ren, H.-L., and F.-F. Jin (2011), Nino indices for two types of
ENSO, *Geophys. Res. Lett.*, 38, doi:10.1029/2010GL046031.
Weng, H., S. K. Behera, and T. Yamagata (2009), Anomalous
winter climate conditions in the Pacific rim during recent El
Niño Modoki and El Niño events, *Clim. Dyn.*, 32(5), 663–674,
doi:10.1007/s00382-008-0394-6.
Widger, W. K. (1949), A study of the flow of angular momentum
in the atmosphere, *J. Meteor.*, 6, 292299.

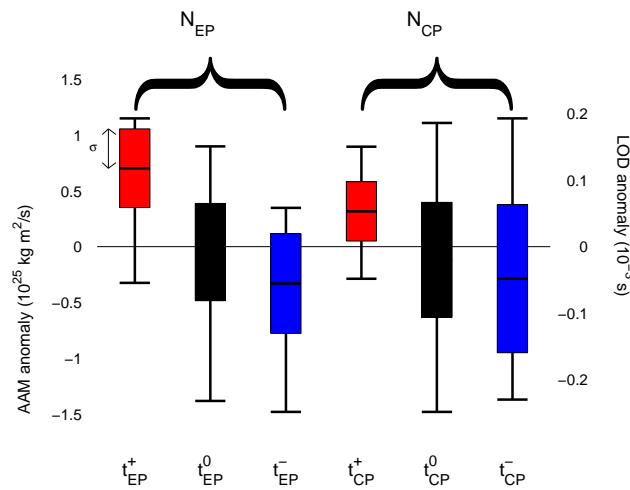


Figure 1. Whisker diagram of the AAM during times where indices (N_{EP} on the left, N_{CP} on the right) are 1- σ above average, below average, or at the neutral state.

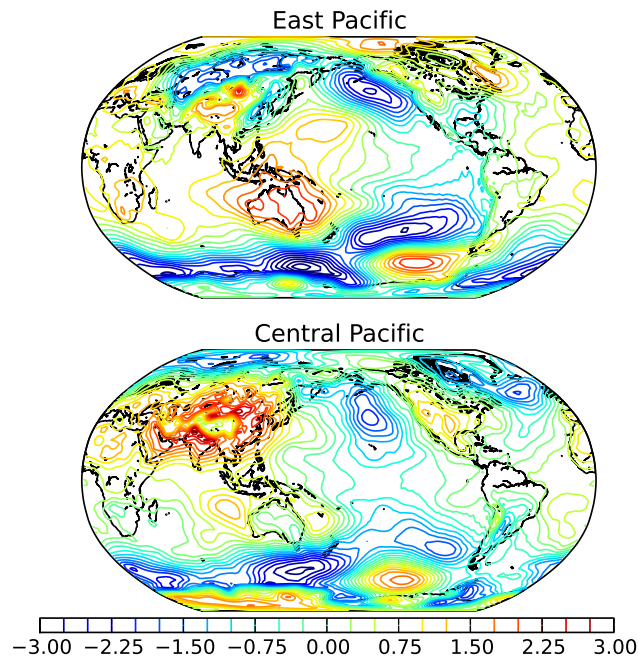


Figure 2. Difference in surface pressure anomaly between positive and negative phase of N_{EP} and N_{CP} , as defined in equation(11).

321 Wolf, W., and R. Smith (1987), Length-of-day changes and moun²⁵ 10.1029/2010GL042810.
 322 tain torque during el niño, *J. of the Atm. Sci.*, 44, 3656–3660.
 323 Yu, J. Y., and S. T. Kim (2010), Three evolution patterns
 324 of Central-Pacific El Nino, *Geophys. Res. Let.*, 37, doi: _____

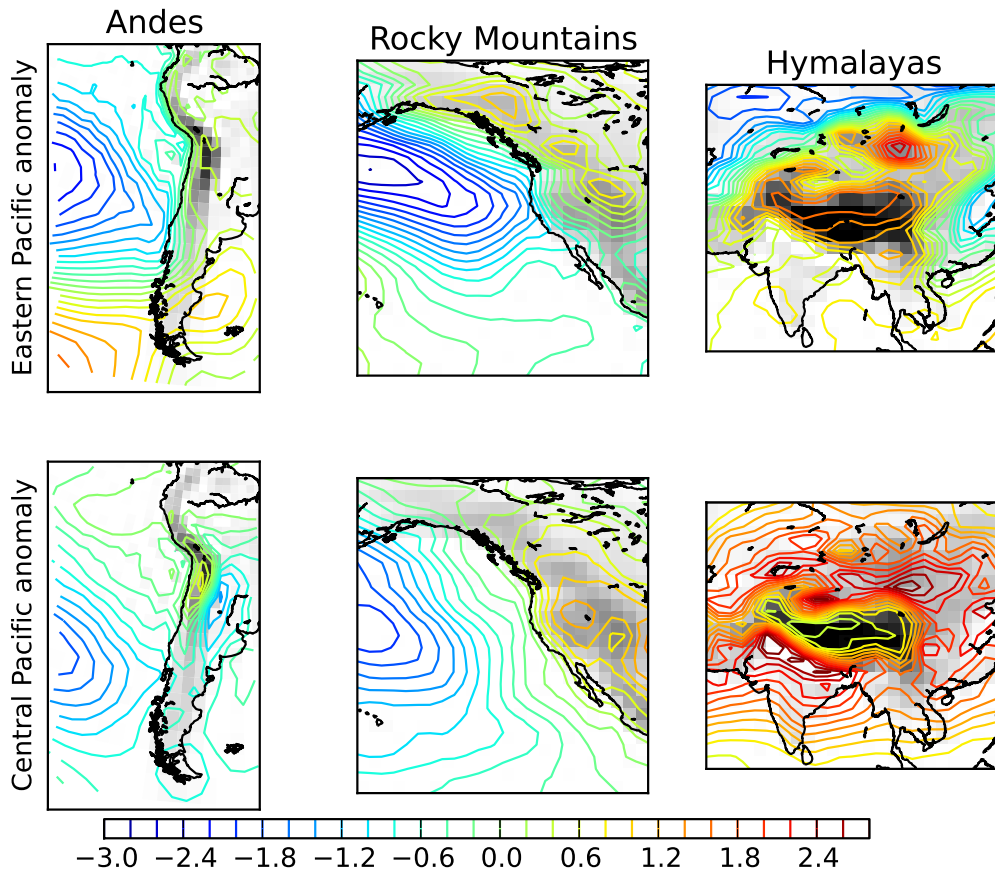


Figure 3. Difference in surface pressure anomaly between positive and negative phase of N_{EP} and N_{CP} , as defined in equation(11), focused on the major mountain ranges (Andes on the left, Rocky Mountains on the center, and Himalayas on the right). The top panel is for EP anomaly and the bottom one for the CP anomaly.

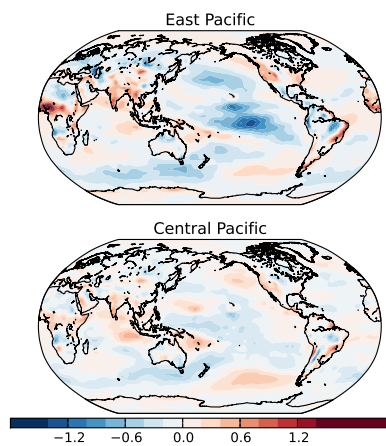


Figure 4. Difference in zonal friction drag anomaly between positive and negative phase of N_{EP} and N_{CP} , as defined in equation(11). The top panels is for the EP anomaly and the bottom one for the CP anomaly.

Table 1. Mountain torque (in Hadley, i.e. 10^{18} Nm), computed from C_{EP} and C_{CP} of the surface pressure, computed as explained by equation (11).

Continent	East Pacific	Central Pacific
Africa	1.2	0.8
Europe	-0.4	0.1
N America	1.7	1.0
S America	1.1	0.0
Asia	1.7	0.2
Oceania	0.2	-0.1
Antarctica	-0.1	0.1
Total	5.4	2.1

Table 2. Friction torque (in Hadley, i.e. 10^{18} Nm), computed from C_{EP} and C_{CP} of the friction drag, computed as explained by equation (11). The separation map for the ocean/continent can be found in Figure 3 of *Marcus et al.* [2011].

Continent/ocean	East Pacific	Central Pacific
Africa	1.2	0.1
Europe	-1.0	-0.1
N America	0.5	0.1
S America	0.0	0.3
Asia	0.1	-0.2
Oceania	-0.2	-0.2
Antarctica	0.5	0.2
N Pac	-2.0	0.2
Eq. Pac	-3.9	-1.3
S Pac	-1.7	-0.3
N Atl	-0.3	-0.4
Eq. Atl	0.3	0.2
S Atl	-1.4	-0.9
Indian	-2.0	-1.1
Antarctic Ocean	0.1	-0.0
Total	-9.9	-3.3